Spectroscopic properties and energy transfer processes in Er^{3+}/Nd^{3+} co-doped tellurite glass for 2.7-μm laser materials

Shan Guan (关　山)[1,2], **Ying Tian (田　颖)**[1,2], **Yanyan Guo (郭艳艳)**[1,2],
Lili Hu (胡丽丽)[1], **and Junjie Zhang (张军杰)**[1*]

[1]*Key Laboratory of Materials for High Power Laser, Shanghai Institute of Optics and Fine Mechanics,*
Chinese Academy of Sciences, Shanghai 201800, China
[2]*Graduate University of Chinese Academy of Sciences, Beijing 100049, China*
Corresponding author: jjzhang@mail.siom.ac.cn

Intense 2.7-μm emissions are obtained from Er^{3+}/Nd^{3+} co-doped tellurite glass samples under the 808-nm laser diode excitation. According to the absorption spectra, Judd-Ofelt parameters and radiative transition probabilities are calculated and analyzed using the Judd-Ofelt theory. The spectroscopic properties and energy transfer mechanism between Er^{3+} and Nd^{3+} are analyzed. The effects of OH^- content on the spectroscopic properties of Er^{3+}/Nd^{3+} co-doped samples are discussed. The obtained results indicate that Er^{3+}/Nd^{3+} co-doped tellurite glass can significantly develop optical properties of 2.7-μm emission, if OH^- groups can be effectively eliminated.

OCIS codes: 160.5690, 160.2750, 160.3380, 300.2140.

doi: 10.3788/COL201210.071603.

Over the past several decades, the increasing demand of potential applications in medicine, remote chemical sensing, the military, and laser surgery, among others, has given rise to the necessity of investigating optical properties in the wavelength region around 2.7 μm[1−5].

Among various rare earth ions, Er^{3+} has played an important role due to the interesting $^4I_{11/2} \rightarrow {}^4I_{13/2}$ transition. However, the quantum efficiency of this transition is rather low in most glass matrices because the energy gap between the $^4I_{11/2}$ and $^4I_{13/2}$ levels is much lower, resulting in the large nonradiative transition probability of $^4I_{11/2}$[6,7]. To obtain high luminescent efficiency, low phonon energy glass hosts are required. Thus, previous efforts have been mainly focused on non-oxide types of glass, such as fluoride, chalcogenide, and some crystal[8−16]. However, according to previous research[17,18], a family of tellurite glass shows promise as host material for rare-earth doping because of ideal glass stability and durability as well as relatively low phonon energy (700 cm^{-1}). Meanwhile, to obtain intense 2.7-μm emission, the suitable co-doping of rare-earth ions is required to increase the pumping efficiency of laser diodes via energy transfer. Many rare-earth ions, such as Yb^{3+}, Ho^{3+}, Pr^{3+}, Tm^{3+}, and Nd^{3+}, have been co-doped with Er^{3+} as sensitizer ions to take advantage of the 2.7-μm emission[19−24].

OH^- groups can greatly affect the optical transmission loss in types of glass. Previous studies have also shown that OH^- groups greatly influence the non-radiative transition of Er^{3+}; OH^- groups are among the important quenching centers in glass hosts[25,26]. Therefore, this work chooses tellurite glass as host matrix to dope with Er^{3+}/Nd^{3+}. Judd-Ofelt parameters and radiative transition probabilities are calculated and discussed based on the absorption spectra using the Judd-Ofelt theory. Moreover, emission properties, energy transfer processes between Er^{3+} and Nd^{3+}, and the effect of OH^- groups are investigated systemically.

The investigated glass has the molar composition of $(69-x)TeO_2$-$20ZnO$-$10Na_2CO_3$-$1Er_2O_3$-xNd_2O_3(x=0, 0.25, 1, and 2). The samples were prepared using high-purity powders of TeO_2, ZnO, Na_2CO_3, Er_2O_3, and Nd_2O_3. Well-mixed 20-g batches of each sample were placed in a platinum crucible and melted at 850 °C for 30 min. To reduce the OH^- content, drying procedures were applied, and the melting glass was bubbled with high-purity oxygen gas. Samples of $67TeO_2$-$20ZnO$-$10Na_2CO_3$-$1Er_2O_3$-$2Nd_2O_3$ were prepared with no bubbling or 60 min of bubbling, respectively. Then, each melted sample was cast on a preheated steel plate and annealed for several hours at a temperature of 10 °C below the T_g before cooling to room temperature at a rate of 20 °C/h.

The absorption spectra were recorded by a Perkin-Elmer-Lambda 900UV/VIS/NIR spectrophotometer in the range of 300–1 200 nm. The emission spectra were measured with a Triax 320 type spectrometer (Jobin-Yvon Co., France) upon excitation at 808 nm. The infrared transmission spectrum was obtained by a Thermo Nicolet (Nexus FT-IR Spectrometer) spectrophotometer. All measurements were carried out at room temperature.

Figure 1 shows the absorption spectra of the Er^{3+} and Er^{3+}/Nd^{3+} doped tellurite glass samples. All the intrinsic absorption transitions from the ground state to the higher state of Er^{3+} and Nd^{3+} in the region of 300–1100 nm were observed. In the absorption spectra, a strong absorption was observed at around 808 nm in the Er^{3+}/Nd^{3+} co-doped glass, indicating that an 808-nm laser diode can be an efficient excitation source. The absorption coefficient of co-doped samples at around 808 nm was proportional to the Nd^{3+} concentration, as shown in the inset of Fig. 1. With the increment of the Nd^{3+} concentration, the absorption intensities of 808-nm enhanced proportionally. Thus, the Er^{3+}/Nd^{3+} can
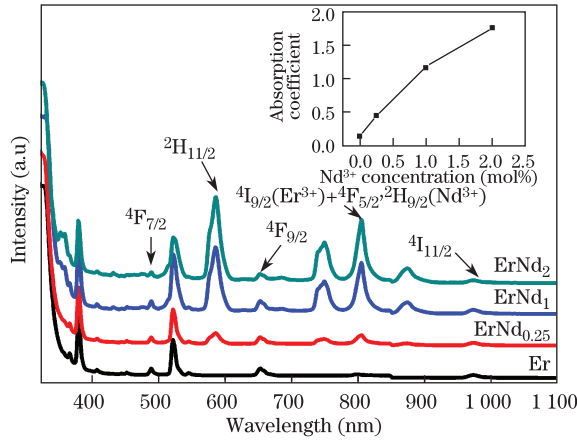
Fig. 1. Absorption spectra of the Er^{3+} and Er^{3+}/Nd^{3+} doped tellurite glass. The inset shows Nd^{3+} concentration dependence of the absorption coefficient at 808 nm.

greatly increase the absorption of the 808-nm pumping light.

To calculate the integrated absorption coefficient for each band, this study used the base glass corrected absorption spectrum. A set of equations, depending on the number of absorption bands considered for the simulation, was generated from the measured electric dipole line strength. By employing the least square fitting method on those equations, the J-O intensity parameters Ω_t ($t = 2, 4, 6$) were attained. The parameters were $\Omega_2 = 9.68 \times 10^{-20}$ cm^2, $\Omega_4 = 1.11 \times 10^{-20}$ cm^2, and $\Omega_6 = 1.89 \times 10^{-20}$ cm^2, respectively, which were similar to those in tellurite systems reported before[27]. The root-mean-square error deviation of the calculated and experimental transition oscillator strength was 0.7×10^{-6}, which was close to that of other reported types of glass[28]. The results verified the reliability of the calculations as well as the validity of the Judd-Ofelt theory for the spectral intensities of Er^{3+} ions.

In general, radiative properties can be predicted by intensity parameters Ω_t. The line strength for an electric-dipole transition (S_{ed}) can be given by[29]

$$S_{\mathrm{ed}} = \sum_{t=2,4,6} \Omega_t |\langle 4f^N(S,L)J \parallel U^{(t)} \parallel 4f^N(S',L')J'\rangle|^2.$$

(1)

Additionally, the line strength for a magnetic-dipole transition (S_{md}) between J manifolds when the transitions subject to the selection rules ($\Delta S = \Delta L = 0$; $\Delta J = \pm 1$ or 0) are represented as

$$S_{\mathrm{md}} = \frac{1}{4m_e^2 c^2} |\langle (S,L) J \parallel L + 2S \parallel (S',L') J'\rangle|^2. \quad (2)$$

Subsequently, the spontaneous transition probabilities are given by

$$A[(S,L)J;(S',L')J'] = A_{\mathrm{ed}} + A_{\mathrm{md}}$$
$$= \frac{64\pi^4 e^2}{3h\lambda^3 (2J+1)} \times \left[\frac{n(n^2+2)^2}{9} S_{\mathrm{ed}} + n^3 S_{\mathrm{md}} \right], \quad (3)$$

where A_{ed} and A_{md} are the electric-dipole transition and magnetic-dipole spontaneous transition probability, respectively.

Furthermore, the fluorescence branching ratios β and radiative lifetimes τ_{rad} can be calculated from

$$\beta[(S,L)J;(S',L')J'] = \frac{A[(S,L)J;(S',L')J']}{\sum_{S',L',J'} A[(S,L)J;(S',L')J']},$$

(4)

$$\tau_{\mathrm{rad}} = \left\{ \sum_{S',L',J'} A[(S,L)J;(S',L')J'] \right\}^{-1}. \quad (5)$$

Using Eqs. (1)–(5) and Ω_t parameters, the spontaneous transition probability (A), total spontaneous transition probability ($\sum A$), radiative lifetime (τ_{rad}), and branching ratios (β) of the optical transitions for the Er^{3+} doped tellurite glass were calculated (Table 1). The predicted spontaneous emission probabilities for $^4I_{11/2} \rightarrow ^4I_{13/2}$ of Er^{3+} was 79.54 s^{-1}, which was higher than those of fluorophosphates (22.16 s^{-1}). A higher spontaneous emission probability generally provides a better opportunity to obtain laser operation. Therefore, the tellurite glass in this work can be a promising host material to achieve 2.7-μm emission based on the $Er^{3+}:^4I_{11/2} \rightarrow ^4I_{13/2}$ transition.

Once the J-O Parameters are known, the radiative properties can be calculated, such as the radiative transition probabilities (A) and branching ratio of the $^4I_{11/2} \rightarrow ^4I_{13/2}$ transition (β), which are also shown in Table 1. The radiative transition rate A and fluorescence

Table 1. Predicted Spontaneous Transition Probability (A), Total Spontaneous Transition Probability ($\sum A$), Branching Ratios (β), and Radiative Lifetimes (Trad) of Tellurite Glass for Various Selected Excited Levels of Er^{3+}

Transition	A(s^{-1})	ΣA(s^{-1})	B(%)	τ
$^4I_{13/2} \rightarrow ^4I_{15/2}$	422.01	422.01	100.00	2.37
$^4I_{11/2} \rightarrow ^4I_{15/2}$	502.47	582.01	86.33	1.72
$^4I_{13/2}$	79.54		13.67	
$^4I_{9/2} \rightarrow ^4I_{15/2}$	188.69	338.23	55.79	2.96
$^4I_{13/2}$	144.92		42.85	
$^4I_{11/2}$	4.62		1.37	
$^4F_{9/2} \rightarrow ^4I_{15/2}$	3 027.23	3 426.76	88.34	0.29
$^4I_{13/2}$	164.20		4.79	
$^4I_{11/2}$	223.20		6.51	
$^4I_{9/2}$	12.13		0.35	
$^4S_{3/2} \rightarrow ^4I_{15/2}$	3 692.26	5 826.39	63.37	0.17
$^4I_{13/2}$	1 868.30		32.07	
$^4I_{11/2}$	111.84		1.92	
$^4I_{9/2}$	153.99		2.64	
$^2H_{11/2} \rightarrow ^4I_{15/2}$	2 4445.45			
$^4F_{7/2} \rightarrow ^4I_{15/2}$	8 058.62			
$^4F_{5/2} \rightarrow$	2 301.44			
$^2H_{9/2} \rightarrow$	3 377.32	10 582.77	0.01	0.09
$^4I_{13/2}$	5 292.79		50.01	
$^4I_{11/2}$	1 723.11		16.28	
$^4I_{9/2}$				
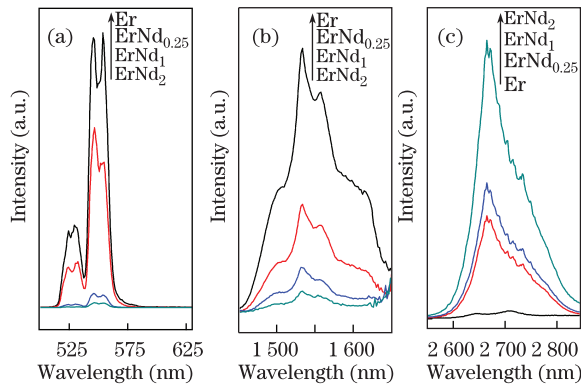
Fig. 2. 550-nm up-conversion and 1.5-μm and 2.7-μm emission spectra of Er^{3+} doped and Er^{3+}/Nd^{3+} co-doped tellurite glass under 808-nm excitation.

branch ratio β of $^4I_{11/2} \rightarrow ^4I_{13/2}$ of Er^{3+} were 79.54 s^{-1} and 13.67%, respectively.

Figure 2(b) shows the 1.5-μm emission spectra pumped by 808 nm. The emission around 1.5-μm was observed as due to the transition of Er^{3+}:$^4I_{13/2} \rightarrow ^4I_{15/2}$. With the increase of the Nd^{3+} doping concentration, 1.5-μm emission intensity decreased obviously. The emission intensity decreased with the further increase of the Nd^{3+} concentration. The same phenomenon can also be observed in Fig. 2(a).

Figure 2(c) shows 2.7-μm emission spectra pumped by 808 nm; the Er^{3+} doped sample is shown to have almost no emission around 2.7 μm. With the increase of the Nd^{3+} concentration, the intensity of the emission at 2.7 μm increased gradually.

Without Nd^{3+} as sensitizer, the Er^{3+}-doped glass presented the very weak intensity of 2.7-μm emission spectra, compared with the strong 550-nm and 1.5-μm emissions. The increase in the content of Nd^{3+} not only led to an enhancement in the 2.7-μm emission but also in the reduction in the 550-nm and 1.5-μm optical emissions, as shown in Fig. 3. As a consequence, Nd^{3+} may be concluded as a suitable sensitizer to enhance the 2.7-μm emission in Er^{3+}-doped tellurite glass. Nd^{3+} ions can obviously enhance the absorption of the pump energy and transfer the energy to Er^{3+} ions. Meanwhile, they could be the quenching center for the 550-nm up-conversion and 1.5-μm emission.

According to the abovementioned absorption and emission spectra, the physical mechanism describing both visible and infrared emissions can be summarized as shown in Fig. 3. Er^{3+} ions were first excited from the ground state to the $^4I_{9/2}$ level by an 808-nm laser. Meanwhile, Nd^{3+} ions were excited directly to the $^4F_{5/2}$ and $^2H_{9/2}$ levels. On one hand, a part of the excited Nd^{3+} ions relaxed non-radiatively to the $^4F_{3/2}$ level. On the other hand, Nd^{3+} ions in the $^4F_{5/2}$, $^2H_{9/2}$, and $^4F_{3/2}$ levels transferred their energy to Er^{3+}:$^4I_{9/2}$ and $^4I_{11/2}$ via the processes $(Nd^{3+}:^4F_{5/2}, ^2H_{9/2} + Er^{3+}:^4I_{15/2}) \rightarrow (Nd^{3+}:^4I_{9/2} + Er^{3+}:^4I_{9/2})$, $(Nd^{3+}:^4F_{5/2}, ^2H_{9/2} + Er^{3+}:^4I_{15/2}) \rightarrow (Nd^{3+}:^4I_{9/2} + Er^{3+}:^4I_{11/2})$, and $(Nd^{3+}:^4F_{3/2} + Er^{3+}:^4I_{15/2}) \rightarrow (Nd^{3+}:^4I_{9/2} + Er^{3+}:^4I_{11/2})$. These energy transfer processes increased the population of Er^{3+}:$^4I_{11/2}$, which led to enhanced 2.7-μm

emission corresponding to $^4I_{11/2} \rightarrow ^4I_{13/2}$. As a result, the increasing population of Er^{3+}:$^4I_{13/2}$ could lead to an increasing 550-nm up-conversion and 1.5-μm emission. However, an obvious decrease was observed in the 550-nm and 1.5-μm emissions, which may be due to the presence of energy transfer channels, such as the following: $(Er^{3+}:^4I_{13/2} + Nd^{3+}:^4I_{9/2}) \rightarrow (Er^{3+}:^4I_{15/2} + Nd^{3+}:^4I_{15/2})$ or/and $(Er^{3+}:^4I_{13/2} + Nd^{3+}:^4I_{15/2}) \rightarrow (Er^{3+}:^4I_{15/2} + Nd^{3+}:^4F_{5/2}, ^2H_{9/2})$. Therefore, the population of Er^{3+}:$^4I_{13/2}$ decreased, which led to a reduction in both 550-nm up-conversion and 1.5-μm emission.

In general, the introduction of OH^- groups in oxide types of glass prepared in air atmosphere cannot be avoided. OH^- content can be determined by the IR spectra. Figure 4 shows the IR spectra of 1 mol% Er^{3+} and 2 mol% Nd^{3+} doped samples with and without 60 min of bubbling. The samples showed a broad, strong absorption at 4.35 and 3.33 μm without bubbling. Absorption bands are commonly attributed to the stretching vibration of OH^- groups. Previous studies showed that the absorption band at 3.33 μm is due to free OH^- groups, while the band at 4.35 μm is attributed to hydrogen-bonded OH^- groups. Thus, the OH^- content in the sample without bubbling oxygen was larger than that in the
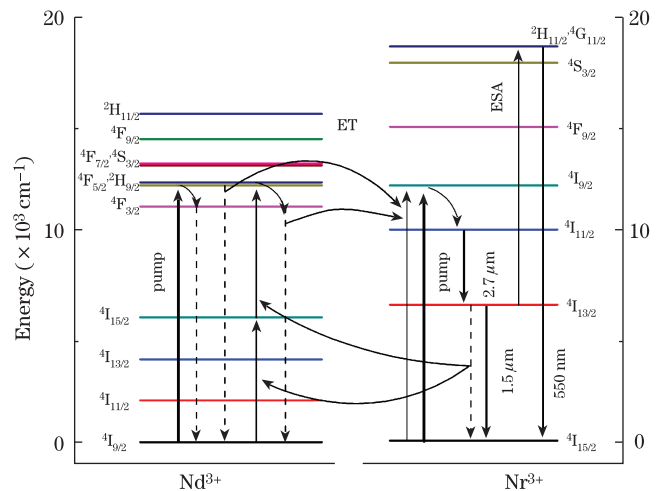
Fig. 3. Energy level diagram of Er^{3+} and Nd^{3+} and the mechanism proposed to explain 550-nm, 1.5-μm, and 2.7-μm emissions.
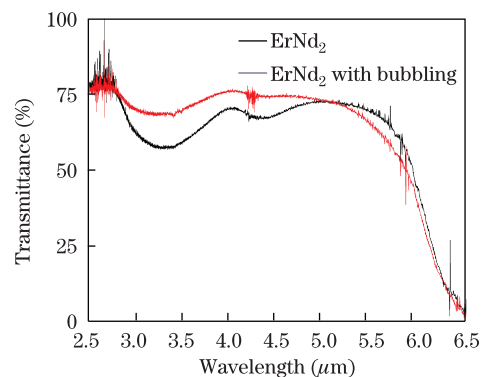
Fig. 4. IR spectra of tellurite glass samples with and without 60 min of bubbling.

samples with bubbling.

The maximum transmittance reached as high as 75%. The 25% loss covered the Fresnel reflections, dispersion, and absorption of the glass. The OH^- groups contained in the glass can be expressed by the absorption coefficient of the OH^- vibration band at 3.33 μm, given by[30]

$$\alpha = \ln(T_o/T)/l, \qquad (6)$$

where l is the thickness of a sample, and T_o and T are the transmitted intensity and incident intensity, respectively. The absorption coefficient of the sample with bubbling α at 3.33 μm was 0.979 cm^{-1}, lower than that without 60 min of bubbling. After bubbling in oxygen, the sample presented better IR transmission property.

According to Ref. [31], the content of the free OH^- groups in glass can be estimated from the measured absorption coefficient at 3.33 μm. The free OH^- group N_{OH} (ions/cm^3) can be obtained by

$$N_{OH} = \frac{N}{\varepsilon \cdot L} \ln \frac{1}{T}, \qquad (7)$$

where N is the Avogadro constant, L is the glass thickness (cm), T is the transmittance, and ε is the molar absorptivity of the free OH^- groups in the glass. The present study adopted the molar absorptivity ε of the free OH^- groups in silicate glass, 49.1×10^3 cm^2/mol[32], given the lack of relevant reports on tellurite glass. Thus, the OH^- concentration in the sample with bubbling was estimated as $N_{OH} = 4.73 \times 10^{19}$ cm^{-3}, an obvious reduction compared with the sample without bubbling ($N_{OH} = 6.89 \times 10^{19}$ cm^{-3}).

Free OH^- is one of the dominant quenching centers in Er^{3+}/Nd^{3+} co-doped glass specimens. According to Ref. [33], two possible energy-transfer mechanisms exist between Er^{3+} ions and free OH^- groups in glass: 1) a small fraction of excited Er^{3+} ions closely bound to free OH^- groups can be quenched rapidly; 2) other excited Er^{3+} ions can transfer the excitation to neighboring non-excited Er^{3+} ions in the first few steps and finally be quenched by free OH^- groups in the transfer route. The latter mechanism should be dominant because most of the excited Er^{3+} ions are not bound with free OH^- groups closely. Therefore, when either the concentration of Er^{3+} ions or the content of free OH^- groups is high enough, the possibility of energy transfer between excited Er^{3+} ions and free OH^- groups can become high; the quenching behavior can then become significant.

According to the considerations of non-radiative processes, the total rate is $1/\tau_m$, which is given by[34]

$$\frac{1}{\tau_m} = A_{rad} + W_{OH} + W_{mp}, \qquad (8)$$

where A_{rad} is the radiative decay rate, equal to the reciprocal of the decay rate in the absence of OH^- groups. W_{mp} is the multiphonon decay rate, and W_{OH} is the energy transfer rate between Er^{3+} and OH^-. The multiphonon relaxation can be considered negligible (<1 s^{-1}) for tellurite glass, which processes relative low phonon energy (700 cm^{-1}). The energy transfer rate between
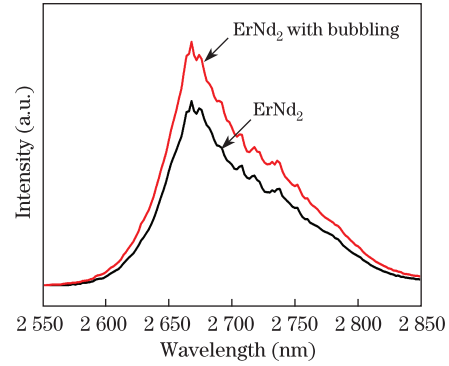
Fig. 5. 2.7-μm emission spectra of 1-mol% Er^{3+} and 2-mol% Nd^{3+} doped samples with and without 60 min of bubbling.

Er^{3+} ions and OH^- groups, W_{OH}, is proportional to the acceptor and donor concentration, and given by

$$W_{OH} = K_{OH-Er} N_{Er} N_{OH}, \qquad (9)$$

where K_{OH-Er} is a constant, as determined by the strength of interactions between Er^{3+} ions and OH^- groups in the case of energy transfer, independent of the concentrations of Er^{3+} and OH^-. N_{Er} is the Er^{3+} concentration (donor concentration), which is a constant in this paper, and N_{OH} is the concentration of the OH^- groups.

According to Eqs. (8) and (9), while at a high OH^- groups concentration, the energy transfer rate between Er^{3+} and OH^- would be higher, which leads to a reduction of the lifetime (τ_m) for the $^4I_{11/2}$ level of Er^{3+} in the sample.

Moreover, the 2.7-μm emission intensity of Er^{3+}/Nd^{3+} co-doped tellurite glass samples with 60 min of bubbling is higher than that without bubbling, as seen in Fig. 5. This result indicates the necessity to remove OH^- groups in the preparation process in order to obtain intense 2.7-μm emission.

In conclusion, intense emission at 2.7 μm is obtained in the Er^{3+}/Nd^{3+} co-doped tellurite glass samples. An enhanced absorption of the 808-nm pumping light with the increasing content of Nd^{3+} is observed. The increasing component of Nd^{3+} not only leeds to an enhancement in the 2.7-μm emission but also in a reduction in the 550-nm and 1.5-μm emissions. The energy transfer mechanisms between Nd^{3+} and Er^{3+} are discussed. The OH^- groups have influences on the IR and the emission spectra. The results prove that the introducing Nd^{3+} to host glass specimens and removing OH^- groups in the preparation process can greatly improve the 2.7-μm emission as well as decrease the 550-nm up-conversion and 1.5-μm emission.

References

1. M. Frenz, H. Pratisto, F. Könz, E.D. Jansen, A. J. Welch, and H. P. Weber, IEEE J. Quantum Electron. **32**, 2025 (1996).

2. D. Hibst, Laser Surg. Med. **12**, 125 (1992).

3. R. Kaufmann and R. Hibst, Clin. Exp. Dermatol. **15,** 389 (1990).

4. R. Allen, L. Esterowitz, and R. J. Ginther, Appl. Phys. Lett. **56,** 1635 (1990).

5. A. Zajac, M. Skorezakowski, J. Swiderski, J. Swiderski, and P. Nyga, Opt. Express **12,** 5125 (2004).

6. S. M. Kirkpatrick, L. B. Shaw, S. R. Bowman, S. Scarles, B. J. Feldman, and J. Ganem, Opt. Express **1,** 78 (1997).

7. M. Pollnau, C. Ghisler, G. Bunea, M. Bunea, W. Luthy, and H. P. Weber, Appl. Phys. Lett. **66,** 3564 (1995).

8. G. J. Kintz, R. Allen, and L. Esterowitz, Appl. Phys. Lett. **50,** 1553 (1987).

9. X. Zhu and R. Jain, Opt. Lett. **32,** 26 (2007).

10. F. Auzel, D. Meichenin, and H. Poignant, Electron. Lett. **24,** 909 (1988).

11. V. K. Tikhomirov, J. Méndez-Ramos, V. D. Rodríguez, D. Furniss, and A. B. Seddon, Opt. Mater. **28,** 1143 (2006).

12. H. Zhong, B. Chen, G. Ren, L. Cheng, L. Yao, and J. Sun, J. Appl. Phys. **106,** 083114 (2009).

13. V. Moizan, V. Nazabal, J. Troles, P. Houizot, J.-L. Adam, J.-L. Doualan, R. Moncorg, F. Smektala, G. Gadret, S. Pitois, and G. Canat, Opt. Mater. **31,** 39 (2008).

14. S. A. Pollack and M. Robinson, Electron. Lett. **24,** 320 (1988).

15. A. S. S. de Camargo, E. R. Botero, E. R. M. Andreeta, D. Garcia, J. A. Eiras, and L. A. O. Nunes, Appl. Phys. Lett. **86,** 241112 (2005).

16. Y. G. Choi, K. H. Kim, and J. Heo, J. Am. Ceram. Soc. **82,** 2762 (1999).

17. L. Gomes, M. Oermann, D. Ottaway, T. Monro, and S. D. Jackson, J. Appl. Phys. **110,** 083111 (2001).

18. M. R. Oermann, H. E. Heidepriem, Y. Li, T. C. Foo, and T. M. Monro, Opt. Express **17,** 15578 (2009).

19. H. Desirena, E. De la Rosa, L. A. Diaz-Torres, and G. A. Kumar, Opt. Mater. **28,** 560 (2006).

20. D. F. de Sousa, L. F. C. Zonetti, M. J. V. Bell, J. A. Sampaio, and L. A. O. Nunes, Appl. Phys. Lett. **74,** 908 (1999).

21. D. F. de Sousa, L. F. C. Zonetti, M. J. V. Bell, R. Lebullenger, A. C. Hernanders, and L. A. O. Nunes. J. Appl. Phys. **85,** 2502 (1999).

22. X. Zhu and R. Jain, Opt. Lett. **33,** 1578 (2008).

23. P. S. Golding, S. D. Jackson, T. A. King, and M. Pollnau, Phys. Rev. B **62,** 856 (2000).

24. B. C. Dickinson, P. S. Golding, M. Pollnau, T. A. King, and S. D. Jackson, Opt. Commun. **191,** 315 (2001).

25. Y. Yan, A. Faber, and H. Waal, J. Non-Cryst. Solids **181,** 283 (1995).

26. E. Snocks, P. G. Kik, and A. Polman, Opt. Mater. **5,** 159 (1996).

27. D. He, J. Zhang, Z. Duan, S. Dai, and L. Hu, Chinese J. Lasers (in Chinese) **32,** 1425 (2005).

28. L. Wen, J. Wang, L. Hu, and L. Zhang, Chin. Opt. Lett. **9,** 12601 (2011).

29. R. Reisfeld and J. Hormadaly, J. Chem, Phys. **64,** 3207 (1976).

30. Z. Li, Z. Chen, and J. Zhang, Acta Opt. Sin. (in Chinese) **4,** 562 (1984).

31. X. Feng, S. Tanabe, T. Hanada, and T. Hanada, J. Am. Ceram. Soc. **281,** 48 (2001).

32. L. Nemec and J. Gotz, J. Am. Ceram. Soc. **53,** 526 (1970).

33. E. Snoeks, P. G. Kik, and A. Polman, Opt. Mater. **5,** 159 (1996).

34. D. C. Yeh, W. A. Sibley, M. Suscavage, and M. G. Drexhage, J. Non-Cryst. Solids **88,** 66 (1986).